RESEARCH ON ADVANCED COMPENSATION CONTROL STRATEGY FOR SOYBEAN COMBINE HARVESTER HEADER HEIGHT BASED ON AREA ARRAY LiDAR
/
基于面阵激光雷达的大豆联合收割机割台高度超前补偿控制策略研究

Qingling LI[1,2], Chao ZHANG[*1,2], Shaobo YE [1,2], Decong ZHENG[1,2]
[1)] College of Agricultural Engineering, Shanxi Agricultural University, Taigu 030801, China;
[2)] Dryland Farm Machinery Key Technology and Equipment Key Laboratory of Shanxi Province, Taigu 030801, China
Corresponding author: Chao Zhang
Tel: +86-152-3541-5968; E-mail: sxndgxyzhangchao@sxau.edu.cn
DOI: https://doi.org/10.35633/inmateh-76-21

Keywords: *Area array LiDAR, soybean combine harvester, header height，Bang-bang control*

ABSTRACT
For the automatic control of soybean harvester header height, this study uses Area array LiDAR for header height detection. An improved quartile range algorithm is used to dynamically remove outliers under crop residue interference. Linear, quadratic, and cubic nonlinear terrain fitting models are established based on the surface undulation characteristics of soybean fields. The Huber loss function is introduced to enhance the robustness of parameter estimation. The balance between model complexity and fitting goodness is quantified using Bayesian information criterion (BIC), and the model intercept term with the smallest BIC value is selected as the terrain reference height. Aiming at the hysteresis characteristics of valve controlled asymmetric hydraulic cylinders, a telescopic dual-mode transfer function model is established, and a Bang-bang switch lead compensation strategy with position threshold is proposed. By predicting the trend of terrain changes, the electromagnetic directional valve is triggered in advance when the height error of the header exceeds the set threshold, effectively reducing the system response delay. Field comparative experiments have shown that at a working speed of 1m/s, the automatic control mode significantly improves the uniformity of cutting compared to the manual mode. When the cutting threshold is set to 20, 25, and 30 mm, the coefficient of variation of cutting height is reduced by 2.13%, 1.71%, and 0.55%, respectively. Moreover, the automatic mode maintains a gentle distribution characteristic within the threshold range of 15-35 mm, verifying the strong robustness and control accuracy advantages of the designed system in complex farmland environments.

摘要
针对大豆收割机割台高度自动控制，本研究采用面阵激光雷达进行割台高度检测，利用改进四分位距算法实现作物残茬干扰下的离群点动态剔除，并依据大豆田地表起伏特征建立线性、二次及三次非线性地形拟合模型，通过引入 Huber 损失函数增强参数估计鲁棒性，结合贝叶斯信息准则（BIC）量化模型复杂度与拟合优度的平衡关系，择优选取 BIC 值最小的模型截距项作为地形基准高度。针对阀控非对称液压缸的迟滞特性，建立伸缩双模态传递函数模型，提出带位置阈值的 Bang-Bang 开关超前补偿策略：通过预判地形突变趋势，在割台高度误差超过设定阈值时提前触发电磁换向阀动作，有效降低了系统响应延迟。田间对比试验表明，在 1m/s 作业速度下，自动控制模式较手动模式显著改善割茬均匀性，当割茬阈值设置为 20、25 及 30mm 时，割茬高度变异系数分别降低了 2.13%、1.71%及 0.55%，且自动模式在 15-35 mm 阈值范围内始终维持平缓分布特征，验证了所设计系统在复杂农田环境中的强鲁棒性与控制精度优势。

INTRODUCTION
The losses during soybean harvesting mainly include header losses, threshing and separation losses, of which header losses account for about 80% of the total losses (*Lian et al., 2024*). Crop cutting and missed cutting are related to the contour and height adjustment of the header. If the position of soybean pods is low, the cutting knife is prone to miss the soybean pods, causing loss of harvest on the cutting platform. If the height of the cutting blade is lowered, it is easy to shovel soil into the cutting table when the blade is in contact with the ground, causing soil to mix with soybean seeds and resulting in "mud flower face" loss, which affects the quality of soybean harvest *(Liu, 2022)*. Therefore, during harvesting, the cutting table should be adjusted in a timely manner according to the height of the soybean bottom pod to achieve cutting table imitation. At present, the detection methods for the height of the cutting table can be basically divided into contact and non-contact methods. For the contact detection method, the Cleodolphi team introduced a position sensor in the height detection of the harvester chassis and used a pressure sensing system to provide real-time feedback on the contact status of the cutter head with the ground (*Cleodolphi et al., 2017*). The combine harvester header

adjustment system developed by Liao Yong achieves dual sensor collaborative detection, capturing crop height information through E18-D80NK infrared diffuse reflection photoelectric sensor, and accurately obtaining header height data with KTC pull rod potentiometer displacement sensor (*Liao et al., 2018*). Li Zerui improved the traditional cutting table system for soybean harvesting characteristics, and designed a floating cutter that achieved adaptive adjustment within a small range through mechanical profiling (*Li et al., 2022*). Zhou developed an intelligent cutting platform system based on angle sensing for the special cultivation mode of soybean under film mulching drip irrigation in Xinjiang. Field test data showed that the relative error of height detection of the device remained stable within 5% (*Zhou et al., 2024*). Non-contact surface parameter detection mainly includes ultrasonic waves, machine vision, infrared sensing, etc. Pasi et al constructed a soil wheel multi ultrasonic sensor fusion measurement system, which controlled the terrain contour detection error within ± 10 mm through multi-source data fusion algorithm (*Pasi et al., 2015*). The ultrasonic dynamic plant measurement system has been validated through orthogonal experiments, and its measurement accuracy is significantly improved compared to traditional floating wheel devices (*Chang et al., 2016*). Huang Yiqi's team proposed a 3D coordinate reconstruction method based on Otsu adaptive thresholding algorithm, which achieved sub centimeter level (MAE<3 mm) terrain detection accuracy through feature point cloud spatial registration (*Huang et al., 2017*). Huang Min proposed a sugarcane ridge height detection scheme based on frequency modulated continuous wave radar. The device can maintain a maximum error level of 3.02 cm under complex working conditions with a vegetation cover thickness of 10 cm and a detection distance of 170 cm (*Huang et al., 2021*). Its penetrating detection mechanism provides an innovative solution for terrain measurement under vegetation cover conditions.

However, the above-mentioned technical systems generally adopt a discrete single point sampling mechanism, which makes the measurement data susceptible to local random noise interference and unable to accurately characterize the macroscopic terrain characteristics of the work area. Based on this, this study proposes a terrain perception system based on area array LiDAR, which uses fusion point cloud feature extraction and introduces a Bang-bang switch advance compensation strategy with position threshold: when the terrain undulation is detected below the preset threshold, the system state remains stable, and only triggers hydraulic actuator adjustment when significant terrain changes are identified.

MATERIALS AND METHODS

Data acquisition and processing of area array LiDAR

This study used Nooploop's TOFSense-MS surface array LiDAR for header height detection, with a ranging range of 1.5c m ~ 4 m and a distance resolution of 1 mm. The data was transmitted through UART interface using NLink protocol, and an 8 × 8 spatial height matrix was constructed in real time to generate a three-dimensional point cloud map. To address the issue of data anomalies caused by crop residues, terrain changes, and sensor noise in the work environment, an improved quartile range algorithm is adopted for outlier detection:

$$Q_1 = P_{25}(h), \quad Q_1 = P_{75}(h), \quad IQR = Q_3 - Q_1 \tag{1}$$

Keep the data range as [Q1-1.5IQR, Q3+1.5IQR], and remove outliers outside the range. Establish three types of terrain fitting models based on the surface topography characteristics of soybean fields:

Linear model:

$$h = \beta_0 + \beta_1 x + \beta_2 y + \varepsilon \tag{2}$$

Quadratic model (including curvature term):

$$h = \beta_0 + \sum_{k=1}^{2}(\beta_k x^k + \gamma_k y^k) + \beta_3 xy + \varepsilon \tag{3}$$

Third order model (high-order nonlinearity):

$$h = \beta_0 + \sum_{k=1}^{3}(\beta_k x^k + \gamma_k y^k) + \beta_4 xy + \beta_5 x^2 y + \beta_6 xy^2 + \varepsilon \tag{4}$$

Among them, (x, y) are the coordinates of the LiDAR array, ε is the residual term, and the model complexity dynamically adjusts with the complexity of the crop field terrain. Huber loss function is used for anti-interference parameter estimation:

$$\min_{\beta}\sum_{i=1}^{n}\rho(\frac{r_i}{\sigma}),\rho(r)=\begin{cases}0.5r^2 & |r|<c\\ c|r|-0.5c^2 & |r|>c\end{cases} \quad (5)$$

The applicability of the model is evaluated based on Bayesian Information Criterion (BIC):

$$BIC = n\ln(\hat{\sigma}^2)+k\ln(n) \quad (6)$$

In the formula, n is the effective data amount, K is the number of model parameters and $\hat{\sigma}^2$ is the robust regression residual variance. The model with the lowest BIC value is selected, and the intercept term of this model is extracted as the fused height value. The left image below displays the original sensor data, which contains four noticeable outlier points. After processing using the method described above, the influence of these anomalies is effectively mitigated.

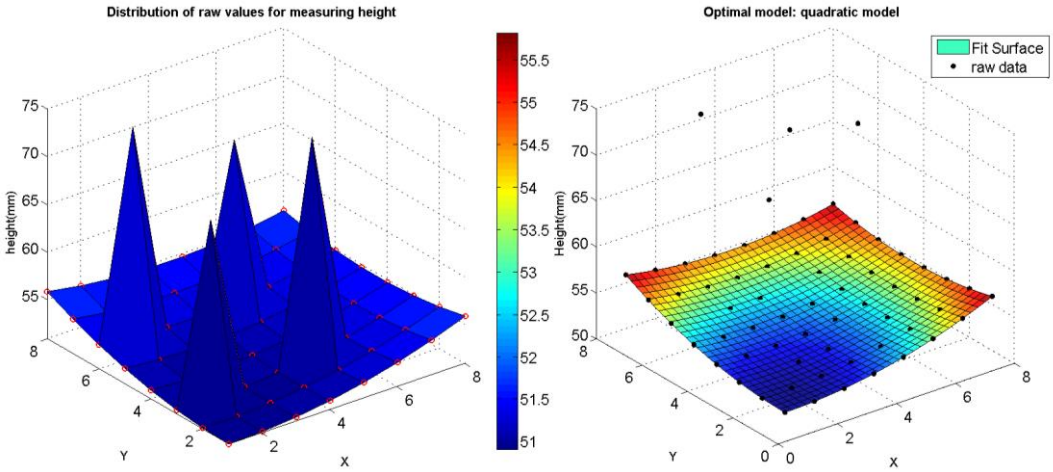

Fig. 1 - Comparison of Front and Rear Processing of Area Array LiDAR Data

Figure 2 illustrates a closed-loop position control system based on the STM32F103ZET6 development board. TOFSense-MS LiDAR data is transmitted to the STM32 master control unit via serial communication. The microcontroller executes control algorithms to drive the H-bridge module, thereby regulating the on/off states and fluid direction of the electromagnetic directional valve, which ultimately achieves header height adjustment. The serial port screen provides a Human-Machine Interface (HMI) supporting parameter configuration, real-time data monitoring, and status display functions.

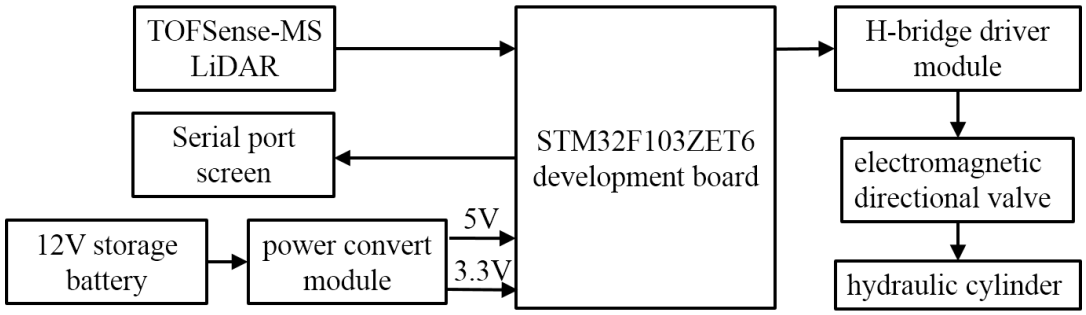

Fig. 2 - Closed-loop position control system

Modeling and analysis of valve controlled asymmetric cylinder system

The height adjustment of the cutting table adopts an asymmetric hydraulic cylinder as the execution unit, and the lifting control is achieved by an electromagnetic directional valve. Compared to proportional valve systems, electromagnetic directional valves have significant engineering applicability in the field of agricultural equipment due to their simple structure, low maintenance costs, and strong resistance to pollution. However, its discrete switch control characteristics result in inherent delay in valve core switching, directly affecting the dynamic response performance of the hydraulic cylinder. To optimize the control accuracy of the system, it is necessary to establish a dynamic model of the valve controlled asymmetric cylinder. The structural diagram is shown in Fig 3.

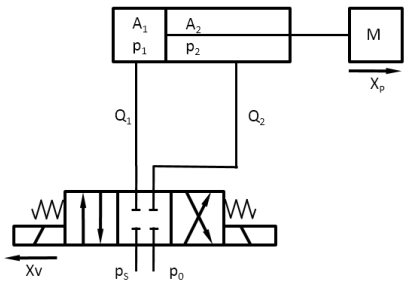

Fig. 3 - Structural diagram of valve controlled asymmetric cylinder system

Assuming the ratio of the two cavity areas is n, that is:

$$n = \frac{A_2}{A_1} \tag{7}$$

Define the load pressure as P_L and the load flow rate as Q_L. When the hydraulic cylinder enters steady state, there are:

$$p_L = \frac{p_1 A_1 - p_2 A_2}{A_1} = p_1 - n p_2 \tag{8}$$

$$Q_L = Q_1 = \frac{Q_1 + n Q_2}{1 + n^2} \tag{9}$$

Due to the different open-loop gains of the extension and retraction of asymmetric hydraulic cylinders, it is necessary to establish basic equations for each case separately. The linear equation for the flow rate of a four-way valve controlled asymmetric cylinder is as follows (*Ye et al., 2015*):

$$Q_L = K_q x_v - K_c p_L \tag{10}$$

$$K_q = \frac{\partial Q_L}{\partial x_v} = \begin{cases} K_{q1} = C_d w \sqrt{\frac{2}{\rho} \frac{(p_s - p_L)}{1 + n^3}}, & x_v > 0 \\ K_{q2} = C_d w \sqrt{\frac{2}{\rho} \frac{n p_s + p_L}{1 + n^3}}, & x_v < 0 \end{cases} \tag{11}$$

$$K_c = -\frac{\partial Q_L}{\partial p_L} = \begin{cases} K_{c1} = C_d w x_v \sqrt{\frac{1}{2\rho} \frac{1}{(1 + n^3)(p_s - p_L)}}, & x_v > 0 \\ K_{c2} = C_d w x_v \sqrt{\frac{1}{2\rho} \frac{1}{(1 + n^3)(n p_s + p_L)}}, & x_v < 0 \end{cases} \tag{12}$$

In the formula: C_d is the valve port flow coefficient; ω is the gradient of the throttle area of the solenoid valve; X_v is the displacement of the reversing valve core; p_1 is the rodless chamber pressure; p_2 is the rodless chamber pressure; P_S represents the fuel supply pressure; ρ represents the density of hydraulic oil.

Assuming that the initial volumes of the two chambers of the piston are the same and the leakage is ignored, the flow continuity equation can be derived:

$$Q_L = A_1 \frac{dx_p}{dt} + \frac{V_t}{2(1 + n^2)\ \beta_e} \frac{dp_L}{dt} \tag{13}$$

$$A_1 P_L = m \frac{d^2 y}{dt^2} + B_c \frac{dy}{dt} + K y + F \tag{14}$$

$$x_p = \frac{A_1 K_q x_v - (K_c + \frac{V_t}{2(1 + n^2)\beta_e} s) F}{(K_c + \frac{V_t}{2(1 + n^2)\beta_e} s)(m s^2 + B_c s + K) + A_1^2 s} \tag{15}$$

Neglecting elastic load, viscous damping, and external load forces, it can be obtained:

$$x_p = \frac{A_1 K_q x_v}{(K_c + \frac{V_t}{2(1+n^2)\beta_e} s)(ms^2) + A_1^2 s} = \frac{\frac{K_q}{A_1} x_v}{s(\frac{V_t m}{2A_1^2(1+n^2)\beta_e} s^2 + \frac{K_c m}{2A_1^2} s + 1)} \quad (16)$$

Table 1

Valve-controlled asymmetric cylinder power structure parameters

Parameter Name	Symbol	Parameter Value	Parameter Name	Symbol	Parameter Value
Effective area of rodless cavity	A_1	1.2566×10^{-3}m^2	Discharge Coefficient	C_d	0.61
Effective area of rod cavity	A_2	0.8765×10^{-3}m^2	Area gradient	ω	0.0047
Area ratio	n	0.6975	Liquid elastic modulus	β_e	6.85×10^{8}Pa
Energy pressure	P_s	8×10^{6}Pa	Oil density	ρ	850kg/m^3
Return oil pressure	P_0	0	Effective volume	V_t	1.2566×10^{-4}m^3

According to the technical manual, the opening time of the 4WE6J61B solenoid valve is 20-45 ms and the closing time is 10-25 ms, both of which are 25 ms. Other parameter settings are shown in Table 1. Therefore, the transfer function when the hydraulic cylinder is extended can be:

$$H_1(S) = \frac{271.0481}{5.8613\times10^{-6}s^3 + 0.001s^2 + s} e^{-0.025s} \quad (17)$$

Similarly, the transfer function when the hydraulic cylinder retracts is:

$$H_2(S) = \frac{226.3698}{5.8613\times10^{-6}s^3 + 0.0012s^2 + s} e^{-0.025s} \quad (18)$$

Analysis of Bang-Bang switch lead compensation strategy with position threshold

The input of an electromagnetic directional valve can be represented as the set $U=\{U+, 0, U-\}$, corresponding to the hydraulic cylinder rising, holding, and falling respectively. Set the height of the header as $h_0(t)$, measure the height value of the sensor as $h(t)$, and the header elevation error e is defined as $h_0(t) - h(t)$. When | e | is less than the position threshold ε, the electromagnetic directional valve does not operate. When e is greater than the position threshold ε, it indicates that the ground elevation increases and the header position is lower, and the header needs to rise. When e is less than the position threshold - ε, it indicates that the ground elevation decreases and the header position is higher, and the header needs to descend. The algorithm flow chart is shown in Fig. 4.

The control algorithm expression is:

$$U = \begin{cases} U_+ & e > \varepsilon \\ 0 & |e| < \varepsilon \\ U_- & e < -\varepsilon \end{cases} \quad (19)$$

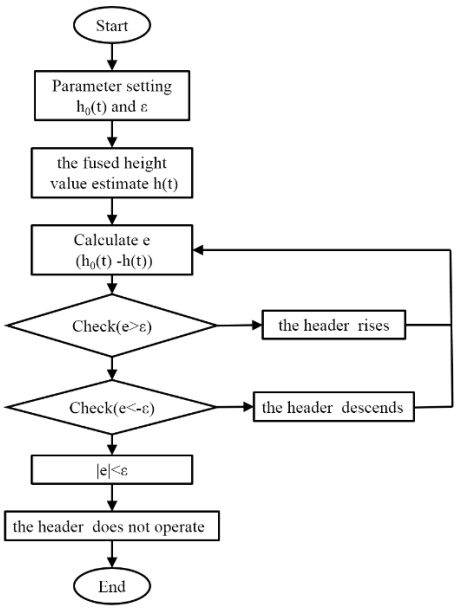

Fig. 4 - Algorithm flow chart

Set the header height to 20 cm and simulate ground height changes using a filtered white noise time-domain road input model, the expression is as follows (*Li et al., 2016*):

$$\dot{q}(t) = -2\pi n_{00} u q(t) + 2\pi n_0 \sqrt{G_q(n_0) u} W(t) \tag{20}$$

In the formula, n_{00} is the lower cut off spatial frequency, taken as 0.011m^{-1}; u is vehicle speed; $q(t)$ is random elevation displacement for road surface; n_0 is reference spatial frequency; $G_q(n_0)$ is the roughness coefficient of the road surface; W(t) is Gaussian white noise with a mean of 0.

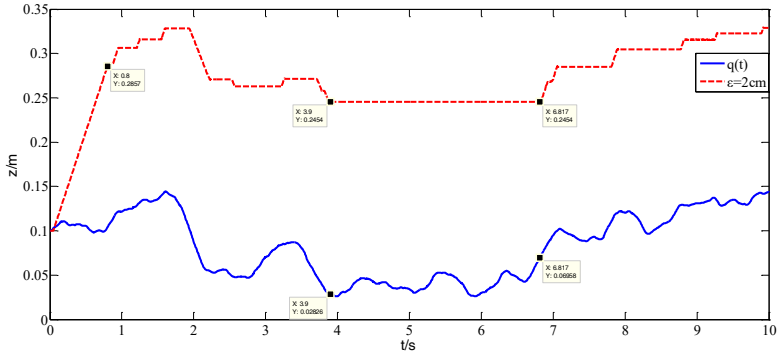

Fig. 5 - Ground elevation (random variation) and cutting height curve

Matlab is used to simulate the variation of the header height and the results are shown in Fig. 5. The position threshold ε is selected as 20 mm. During the time period of 0-0.8 s, due to the fact that the header height is less than 20 cm above the ground, the hydraulic cylinder rises. From 3.9 to 6.817 s, although the ground elevation changes between 2.8 cm and 6.9 cm, the magnitude of the change does not exceed the threshold. At this time, the header height remains at 24.54 cm and does not move. Overall, it shows a control effect of not adjusting the small undulating road surface, and only adjusting it for large undulations.

Field experiment testing

A comparative experiment of soybean harvesting was conducted at the Taigu Shenfeng Experimental Base. The experiment set up a manual and automatic dual-mode control group. The cutting height was used to invert the dynamic changes in the cutting table height, with a constant operating speed of 1 m/s, a preset cutting height of 200 mm, and a working interval length of 30 m. In manual mode, the cutting height will remain at the preset value and will not be adjusted in real-time during the operation process. In automatic mode, the cutting threshold is set to 15 mm, 20 mm, 25 mm, 30 mm, and 35 mm respectively.

Extract 50 sets of cutting height samples continuously from the stable operation section of the harvester, and select the average cutting height and cutting height coefficient of variation (CV). The kurtosis coefficient k is used as a measurement indicator, and its calculation formula is as follows:

(a) Soybean Harvest Experiment (b) Measurement of cutting height

Fig. 6 - Field experiment on height control of soybean sun cutting machine cutting table

$$\bar{L} = \frac{\sum_{i=1}^{n_1} L_i}{n_1} \tag{21}$$

$$C.V = \frac{\sqrt{\sum_{i=1}^{n_1}(L_i - \bar{L})^2}}{\bar{L}} \tag{22}$$

$$k = \frac{n(n+1)\sum_{i=1}^{n_1}(L_i - \bar{L})^4 - 3[\sum_{i=1}^{n_1}(L_i - \bar{L})^2]^2(n-1)}{(n-1)(n-2)(n-3)s^4} \tag{23}$$

In the formula: n_1 is the total number of measured cuttings; L_i is the i-th measurement of cutting height, mm; m_i is the i-th weighing mass, kg.

RESULTS

Some measurement data are shown in Table 2, and the distribution of cutting height is shown in Fig. 7.

Table 2

Measurement values of cutting height (top 10 groups)

Cutting threshold / mm	Measurement point cutting height /mm									
	1	2	3	4	5	6	7	8	9	10
15	175	180	175	190	200	170	190	220	220	225
20	190	200	185	210	185	210	210	200	195	200
25	198	220	200	180	200	180	190	200	220	180
30	210	180	210	180	185	230	195	220	190	195
35	200	190	185	190	200	220	180	190	180	210
Manual mode	195	205	200	195	215	185	200	190	195	185

The experimental data processing results are shown in Table 3. In manual mode, the absolute error between the average cutting height and the preset cutting height is less than 8 mm, while in automatic mode it is reduced to 5 mm. Compared with manual mode, when the cutting threshold is set to 20, 25, and 30 mm, the coefficient of variation of cutting height is reduced by 2.13%, 1.71%, and 0.55%, respectively. The kurtosis coefficient analysis further reveals that manual mode presents a peak distribution (kurtosis=3.4635), while automatic mode maintains a gentle distribution feature within the threshold range of 15-35 mm (kurtosis interval: -1.2306 to -0.6541), indicating that the system effectively suppresses the occurrence of extreme deviation values.

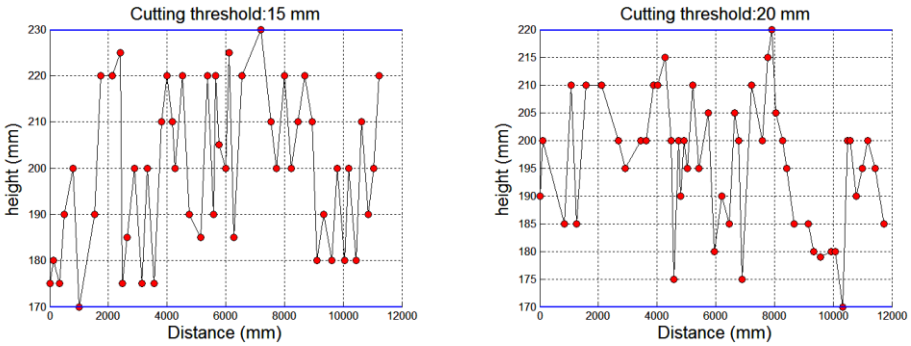

（a）The cutting threshold is 15 mm （b）The cutting threshold is 20 mm

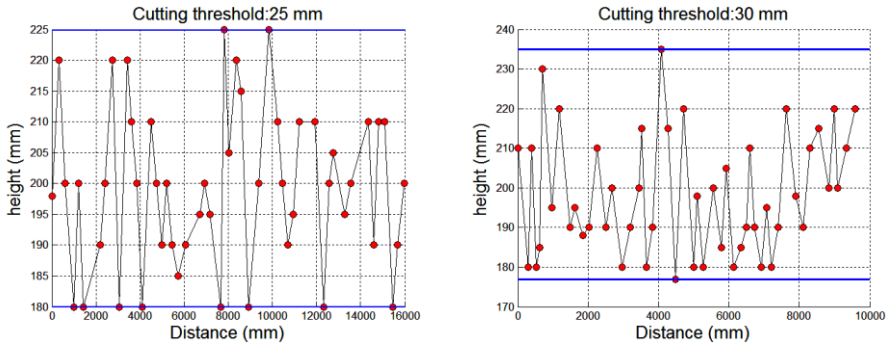

（c）The cutting threshold is 25 mm （d）The cutting threshold is 30 mm

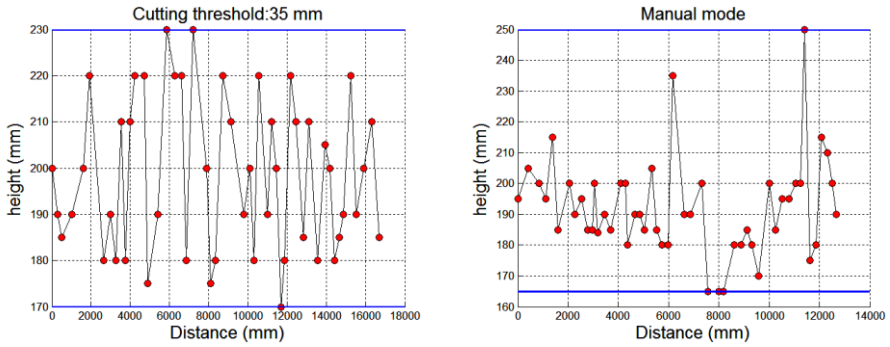

（e）The cutting threshold is 35 mm （f）Manual mode

Fig. 7 - Distribution of cutting height

Table 3

Analysis of Experimental Data Processing Results

Cutting threshold / mm	Average cutting height $\bar{L}$	Coefficient of variation of cutting height C.V / %	Kurtosis coefficient
15	199.7	8.49%	-1.2306
20	195.88	6.04%	-0.6541
25	199.36	6.46%	-0.701
30	198.12	7.62%	-0.6658
35	198.3	8.35%	-1.1811
Manual mode	192.08	8.17%	3.4635

CONCLUSIONS

(1) By integrating the high-resolution 3D terrain detection capability of Nooploop TOFSense-MS area array LiDAR, combined with an improved quartile range algorithm, outliers caused by interference sources such as crop residues and sensor noise are dynamically removed. Linear, quadratic, and cubic terrain fitting models are constructed based on Huber robust regression framework. By quantifying the trade-off between model complexity and terrain adaptability using Bayesian Information Criterion (BIC), the intercept term with the smallest BIC value is selected as the reference height to achieve accurate representation of complex farmland terrain.

(2) Aiming at the nonlinear hysteresis characteristics of valve-controlled asymmetric hydraulic cylinder systems, a telescopic dual-mode transfer function model is established, and a Bang-Bang switch lead compensation strategy based on position threshold is proposed. By predicting the trend of terrain changes, the electromagnetic directional valve is triggered to act in advance.
(3) Field comparative experiments show that at a working speed of 1 m/s, the coefficient of variation of cutting height in automatic control mode is significantly reduced compared to manual mode (when ε=20mm, C.) V=6.04%，The automatic mode maintains a gentle distribution feature within the threshold range of 15-35 mm, with a decrease of 26.1%. The research results provide theoretical support and engineering practice paradigm for intelligent control of high-precision agricultural equipment, which can be further extended to the optimization of imitation systems in multi crop harvesting scenarios such as corn and wheat.

ACKNOWLEDGEMENT

This research was funded by the Scientific and Technological Innovation Programs of Higher Education Institutions in Shanxi (No.2022L096) and the Youth Science and Technology Innovation Project of Shanxi Agricultural University (No.2020QC12), the National Key R&D Program of China (2021YFD1600602-09).

REFERENCES

[1] Chang K., Zaman, Q .(2016). An on-the-go ultrasonic plant height measurement system (UPHMS II) in the wild blueberry cropping system. *ASABE Annual International Meeting.* 162460289. DOI:10.13031/aim.20162460289.
[2] Wang Y., Zhang G., Qian X., Dong Q. (2025). Semi-physical simulation research on the control system of combine harvester cutting table [J]. *INMATEH - Agricultural Engineering*, Vol.75, Issue 01, pp.797-808,https://doi.org/10.35633/inmateh-75-68.
[3] Huang M., Li G. (2021). Detection of Ridge Height in Sugarcane Fields Based on Linear Frequency Modulation Continuous Wave Radar (基于线性调频连续波雷达的甘蔗垄高检测). *Journal of Southwest University*, Vol.43, Issue 02, pp. 31-39, https://doi.org/10.13718/j.cnki.xdzk.2021.02.005.
[4] Huang Y., Huang T., Yang R. (2017). Detection and test of sugarcane cutting height based on machine vision.（基于机器视觉的甘蔗切割高度检测与试验）. *Journal of Chinese Agricultural Mechanization*, Vol.38, Issue 09, pp.81-87. https://doi.org/10.13733/j.jcam.issn.2095-5553.2017.09.017.
[5] Li Z., Huang J., Liu Y. (2016). Modeling and simulation on white noise of road roughness in time domain (白噪声路面不平度时域模型的建立与仿真). *Journal of Jiangsu University(Natural Science Edition)*, Vol.37, Issue 05, pp. 503-506+524. https://doi.org/10.3969/j.issn.1671-7775.2016.05.002.
[6] Li Z. (2022). *Design of soybean profiling header and control system for multi-crop crawler combine harvester (多作物兼用型履带式联合收获机大豆仿形割台设计与调控系统研制).* (Master's thesis). Jiangsu University. ZhenJiang/China. https://doi.org/10.27170/d.cnki.gjsuu.2022.000016.
[7] Liao Y., Xiang X., Wu M., Liu D., Chen Y., Li Y. (2018). Design and test of the adaptive height adjustment system for header of the combine–harvester (联合收割机割台高度自适应调节系统的设计与试验). *Journal of Hunan Agricultural University (Natural Sciences)*, Vol. 44, Issue 3, pp. 326-329. https://doi.org/10.13331/j.cnki.jhau.2018.03.017.
[8] Lian X., Wang J., Zhu Y. (2024). Research status analysis of key technology and loss of soybean harvester header.（大豆收获机割台关键技术及损失研究现状分析）. *Journal of Chinese Agricultural Mechanization*, Vol.45, Issue 08, pp.8-13. https://doi.org/10.13733/j.jcam.issn.2095-5553.2024.08.002.
[9] Liu G. (2022). *Research on Profiling Technology of Soybean CombineHarvester Header (大豆联合收获机割台仿形技术研究).* (Master's thesis). Chinese Academy of Agricultural SciencesThesis. Beijing/China. https://doi.org/10.27630/d.cnki.gznky.2022.000712.
[10] Suomi P. (2015). Automatic working depth control for seed drill using ISO 11783 remote control messages. *Comput. Electron. Agric.*, Vol.116, pp. 30-35. https://doi.org/10.1016/j.compag.2015.05.016.
[11] Ye X. (2015). *Research on Modeling and Control Method of Value-controlled Asymmetrical Cylinder System (阀控非对称缸系统的建模与控制方法研究).* (Doctor's thesis). Hefei University of Technology. Hefei/China. https://doi.org/10.7666/d.Y2925638.
[12] Zhang C., Li Q., Ye S., Zhang J., Zheng D. (2024). Header Height Detection and Terrain-Adaptive Control Strategy Using Area Array LiDAR. *Agriculture*. 14(8):1293. https://doi.org/10.3390/agriculture14081293.